Marine and Petroleum Geology 127 (2021) 104979

Contents lists available at ScienceDirect

Marine and Petroleum Geology

journal homepage: www.elsevier.com/locate/marpetgeo

Diagenetic history vs. thermal evolution of Paleozoic and Triassic reservoir rocks in the Ghadames-Illizi Basin (Algeria-Tunisia-Libya)

Andrea Di Giulio [a], Domenico Grigo [b], Massimiliano Zattin [c], Chiara Amadori [a], Alberto Consonni [b], Chiara Nicola [a], Andrea Ortenzi [b], Paolo Scotti [b], Silvia Tamburelli [a,*]

[a] Department of Earth and Environmental Sciences, University of Pavia, Pavia, PV, Italy
[b] Eni S.p.A, Exploration and Production Division, San Donato Milanese, MI, Italy
[c] Department of Geosciences, University of Padova, Padova, PD, Italy

ARTICLE INFO

Keywords:
Diagenesis
Thermal history
Fluid inclusions
Thermochronology

ABSTRACT

Unravelling the time-space distribution of diagenetic events modifying the pore network of reservoir rocks is fundamental for hydrocarbon research, but it needs to constraint a number of variables driving that distribution along the geological history of sedimentary basins.

Here, we present the results of an integrated study performed on Paleozoic and Triassic reservoir sandstones coming from the Ghadames-Illizi Basin (North Africa), where it is still debated the possible thermal effect on the petroleum system of the Cenozoic magmatic activity occurred in neighbouring regions of the studied basin.

The study aims to contribute in solving that problem by combining: the reconstruction of the relative timing of diagenetic events obtained by petrography; the detection of precipitation temperature of cements from microthermometric analyses of fluid inclusions; the collection of thermal constraints from low-T thermochronology (Fission tracks and (U–Th)/He analyses) on detrital apatite grains; the maturity profile of organic matter obtained through vitrinite reflectance and spore analyses. This integrated approach was applied to samples coming from a basin region where Hercynian erosion was minor, in order to discuss different thermal scenarios, with or without a Tertiary thermal overprint.

The results point out that a simple thermal scenario with heating only due to increasing burial depth is not able to account for the observed experimental data (both organic matter and fluid inclusions data sets); conversely, a Tertiary heating overprint well explain the data collected. Between the tested scenarios considering a Tertiary overheating, the one with an Early Tertiary thermal event seems to fit better data, even though a younger thermal peak is possible. Whatever the case, the choice of the thermal scenario significantly changes the calculated age of cements precipitation in the pore system of the studied reservoir rocks.

1. Introduction

The reconstruction of the diagenetic evolution of reservoir rocks and its impact on their pore network is certainly a fundamental task for hydrocarbon exploration. Nevertheless, it is not always easy to complete that picture, as it needs to constraint a number of variables driving that distribution along the geological history of each specific sedimentary basin, with heat-flow through geologic time probably being the trickiest to challenge.

Here, we present the results of an integrated study performed on Paleozoic and Triassic reservoir rocks from the Ghadames-Illizi Basin, one of the most prolific hydrocarbon regions in North Africa (Wendt et al., 2009; Galeazzi et al., 2010; English et al., 2017b). In that region, it is still debated the possible thermal effect exerted on the basin by the increase of the heat flow related with the Tertiary magmatic activity occurred in the neighbouring regions (e.g. Hoggar Dome; Liégeois et al., 2005; English et al., 2016b) and its consequences on the petroleum system.

In order to contribute to solve this debate, we performed an integrated study in a part of the Ghadames-Illizi Basin where uplift and erosion during the Hercynian orogeny seem to have been relatively minor or even absent, and where post-Hercynian samples are available, thus making possible to better detect the eventual effect of Tertiary overheating. The study was performed through the combination of: i)

* Corresponding author.
E-mail address: silvia.tamburelli01@universitadipavia.it (S. Tamburelli).

https://doi.org/10.1016/j.marpetgeo.2021.104979
Received 22 October 2020; Received in revised form 22 January 2021; Accepted 13 February 2021
Available online 19 February 2021

microthermometric analyses of fluid inclusions trapped in diagenetic minerals; ii) low-T thermochronology (fission-tracks and (U–Th)/He analyses on clastic apatite grains); and iii) vitrinite reflectance and spores maturity analyses. The constraints achieved through this experimental data set were then compared with the predictions regarding the thermal evolution of the studied rocks according to 3 different thermal scenarios, including or excluding a Tertiary overheating, to test which of them better explains the collected data.

According to that approach, we conclude that a Tertiary overheating is necessary to fit experimental data; in addition, between the two tested scenarios including such Tertiary heating (Early vs. Late Tertiary heating) the one occurred during the Early Tertiary (65 Ma) better accounts for experimental evidences, although the Late Tertiary heating cannot be completely excluded. Whatever the case, it is important to note that the predicted geologic age of each phase of cement precipitation, that modified the pore network of studied reservoir rocks, significantly change as a function of the adopted thermal model, and this potentially has relevant consequences on the exploration activity.

2. Geological setting and stratigraphy

The Ghadames-Illizi Basin is one of the sedimentary basins that extend from southern Algeria and Tunisia into Libya in North Africa; it is located in the northern margins of the Precambrian Reguibat (Eglab) Shield (West African Craton) and the Hoggar (Touareg) Shield, and extends principally in Algeria, near other petroleum prolific basins of Tunisia and Libya (Fig. 1). The Ghadames-Illizi Basin is bounded eastward by the Tihemboka and Gargaf Arch, southward by the Hoggar Massif, and to the west by the Amguid-Hassi Touareg structural axis which separates the Ghadames-Illizi Basin from the Mouydir Basin (Fig. 1).

The recoverable reserves of this prolific hydrocarbon province are estimated at around 5 Bbbl oil and 37 Tcf (trillion cubic feet) (1.0 tcm) of gas (Galeazzi et al., 2010), for this reason it is considered one of the most important hydrocarbos reach areas in North Africa.

Since the discovery of enormous hydrocarbon reservoirs in the early '50s, the structural and depositional history of the basin was explored by hundreds of drillings and investigated by several scientific works (Tissot et al., 1973; MacGregor, 1996; Boote et al., 1998; Traut et al., 1998; Galeazzi et al., 2010; English et al., 2016, 2017). Nevertheless, many data collected during this hydrocarbon activity are still reserved and the published papers generally suffer for scarce stratigraphic data, which are often obscured by poorly defined lithostratigraphy, and loose dating from palynomorphs and chitinozoans correlations (Wendt et al., 2009).

Other studies have discussed the burial and thermal history of the Berkine-Ghadames-Illizi area through sonic compaction analysis, thermal maturity, fluid inclusion microthermometry, and apatite fission-track data (English et al., 2016b, 2016c, 2017a; Underdown and Redfern, 2008). These studies confirmed that the preserved Paleozoic sequence in the Illizi Basin was subjected to elevated temperatures in the past, possibly because of additional burial prior to Hercynian exhumation, and afterwards during reburial in the Mesozoic and early Cenozoic. According to these studies, the maximum burial most likely occurred during the Early Eocene, prior to uplift of the Hoggar massif and the northward tilting of the Illizi Basin (English et al., 2016b, 2017a).

From a stratigraphic point of view, the Ghadames-Illizi Basin sedimentary succession starts with a Paleozoic sequence resting upon the eroded pan African basement (Fig. 2).

This Paleozoic sequence begins with upper Cambrian-lower Ordovician sandy fluvial sediments. Subsequent, shallow marine deposition occurred during the Ordovician (Tremadoc to lower Caradoc), recording a period of transgression (Fig. 2). Above this, a eustatic sea-level fall and glacial scouring associated with the short-lived Ashgillian glaciation is recorded by the Ashgillian (or locally termed Taconic) Unconformity (English et al., 2016, 2017a), documenting a period when North Africa was situated near the South Pole.

The following Silurian-Devonian-Carboniferous sequence is prevalently made by continental interbedded sandstones and shale units, with

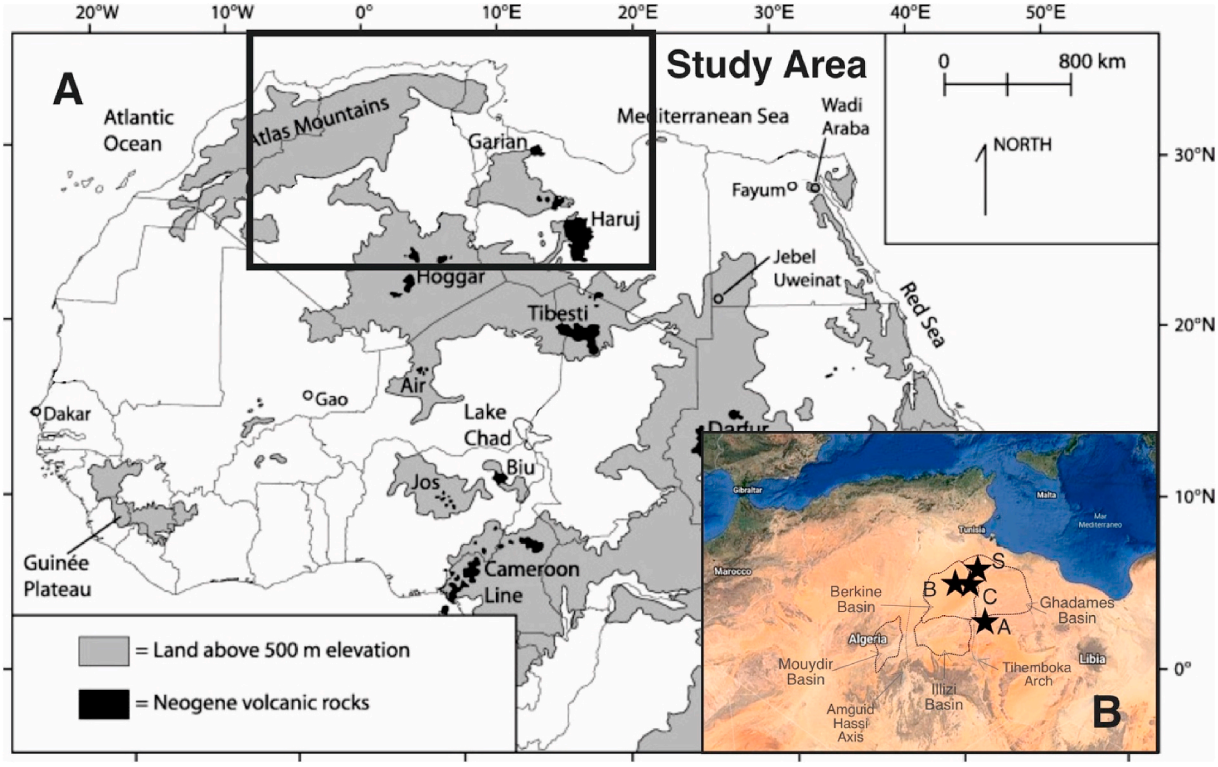

Fig. 1. A) location map of the studied area with magmatic related topographic domes and Neogene volcanic rocks distribution (redrawn after Swezey, 2009); B) location map of the studied wells.

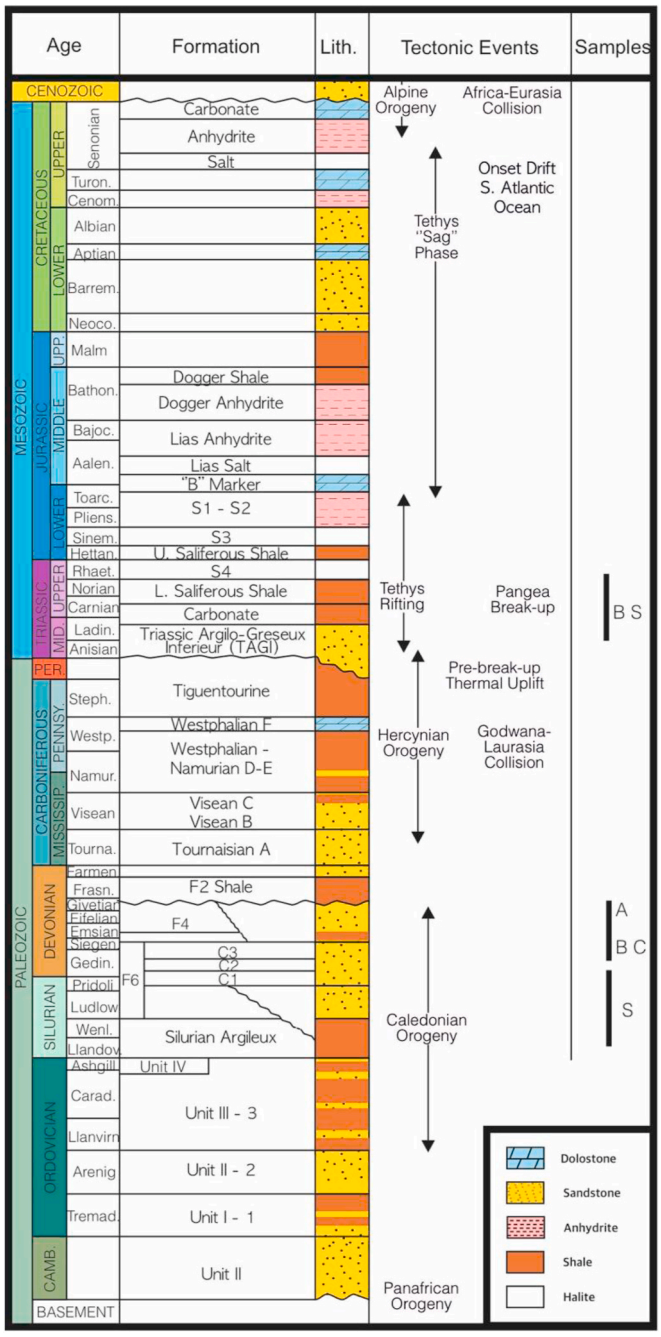

Fig. 2. Generalized stratigraphy of the Ghadames-Illizi Basin and timing of major geodynamic events occurred in the region (redrawn after English et al., 2016). On the right the stratigraphic intervals sampled for the present study are reported; letters refer to different wells whose location is reported in Fig. 1B.

only minor carbonate intervals in the middle Devonian and upper Carboniferous.

During the collision of Gondwana with Laurasia, the Late Carboniferous-Early Permian Hercynian (Variscan) Orogeny caused an extensive uplift of the region and widespread erosion along the north-south trending arches in northwest Africa (Boote et al., 1998; English et al., 2016; Acheche et al., 2001); this caused the erosion of the post-Cambro-Ordovician sequence on some of these uplifted arches, even if in the Ghadames-Illizi Basin the majority of the Paleozoic sequence is still preserved (Galeazzi et al., 2010; English et al., 2016b) (Fig. 2). The Hercynian unconformity of Permian age represents the stratigraphic record of this important orogenic phase, and the burial before it is the first candidate to explain overmaturation of Illizi Basin reservoir rocks with respect to their burial depth.

The opening of the Tethyan seaway was followed by the renewed deposition of the Mesozoic-Early Cenozoic "Tethys Supersequence" (Boote et al., 1998) in North Africa and a Triassic salt basin developed to the north of the Ghadames-Illizi Basin (Galeazzi et al., 2010). In the Illizi-Ghadames region, Mesozoic-Cenozoic deposition was characterized by Early-Mid Aptian transpression and strike-slip deformation during the Austrian event (Galeazzi et al., 2010), and moreover by Mid-Late Eocene inversion that caused also the growth of the Atlas range to the north (English et al., 2016b). Finally, during the Mid-Late Eocene, intraplate magmatism started in North Africa causing uplift and leading to the development of numerous topographic swells and large-scale exhumation of flanking sedimentary basins such as the Illizi and Tim Mersoï Basins (Wilson and Guiraud, 1992; Wilson et al., 1998; Liegeois et al., 2005; English et al., 2016b). Changes in heat flow related to the thermal event that caused this Tertiary magmatism is the other candidate to explain overmaturation of Illizi Basin reservoir rocks with respect to their burial depth.

3. Materials and methods

3.1. Materials

To the aim of the present work, it is also important to stress that the thermal effect of burial pre-dating Hercynian erosion is not easy to decipher where post Hercynian sediments are not preserved, indeed it can be investigated where post-Hercynian sediments are preserved, like in the studied area. Therefore, several samples coming from 3 hydrocarbon wells were selected for optical kerogen analysis in order to provide the maturation profile (vitrinite reflectance and Ro% eq from spores were considered) along the drilled sequences.

In addition, 18 sandstone core samples (courtesy of Eni), selected among a set of 33 samples coming from 4 hydrocarbon wells, were selected for diagenetic events chronology determination and to perform the microthermometric study of fluid inclusions (Table 1; Fig. 3).

The studied data set is completed by 4 samples selected for the thermochronologic study of detrital apatite grains (Table 2; Fig. 3). The stratigraphic age of studied samples varies from Silurian and Devonian (pre-Hercynian) to Triassic (post-Hercynian), and have been sampled at a present-day depth ranging from 2177 to 3870 m below rotary table (Table 1).

3.2. Maturity of organic matter

Thermal maturity data were acquired from cutting and bottom core samples after optical kerogen analysis on plug and slide, although only data of vitrinite reflectance (Ro%) and vitrinite reflectance equivalent from spores were considered (measurement of reflectance on plug).

After washing and drying, 15 or more grams of grinded sample are treated with strong acids (HCl 37% and HF 40%) to eliminate mineral matter. Samples are washed again; for palynological slides, further filtering, centrifugation and treatment with ZnCl2 (1.9 kg/L) and KOH (10%) are used for to break apart the isolated organic matter. The residual kerogen, after washing with distilled water, is mounted on plugs for vitrinite reflectance or slides for kerogen composition analysis.

Plugs are polished and then analyzed in reflected light with a ZEISS MPM 400 and a CRAIC QDI 302 optical microscopes, using oil immersion objectives. The reflectance (Ro%) of all fragments of the vitrinite maceral is measured and then, after identification of the indigenous vitrinite population, a mean value of Ro% is assessed for each sample. The measure of reflectance is also possible directly on the spores (and also on the zooclasts) and the value can be converted into Ro% equivalent (Alpern, 1970; Bertrand, 1990).

Slides are analyzed in transmitted light using a Zeiss Axioplan 2 microscope with 10x, 20x and 40× air objectives. On slides, it is possible

Table 1
Burial depth, stratigraphic age and performed analyses on the samples set of reservoir rocks studied for the present work.

Depth (m) q.t.r	Depth (m) b.s.l.	Sample	Well	Age	FI	AFT	(U–Th)/He
2177	1803	S1	S	Middle Trias	X		
2229.5	1855.5	S2		Middle Trias	X	X	X
2240.7	1866.7	S3		Middle Trias	X	X	X
3001.5	2627.5	S4		Silurian	X		
3002.3	2628.3	S5		Silurian	X		
3468.2	3194.2	C1	C	Lower Devonian	X		
3674.75	3400.75	C2		Lower Devonian	X		
3840.68	3566.68	C3		Lower Devonian	X		
3007.8	2793.8	B1	B	Triassic	X		
3010	2796	B2		Triassic	X		
3014	2800	B3		Triassic	X		X
3015.7	2801.7	B4		Triassic	X		
3830.1	3616.1	B5		Lower Devonian	X		X
3841.3	3627.3	B6		Lower Devonian	X		
3870.1	3656.1	B7		Lower Devonian	X		
2591	1913	A1	A	Middle Devonian	X		
2612–2617	1934–1939	A2		Middle Devonian			X
2619	1941	A3		Middle Devonian	X		
2636	1958	A4		Middle Devonian	X		

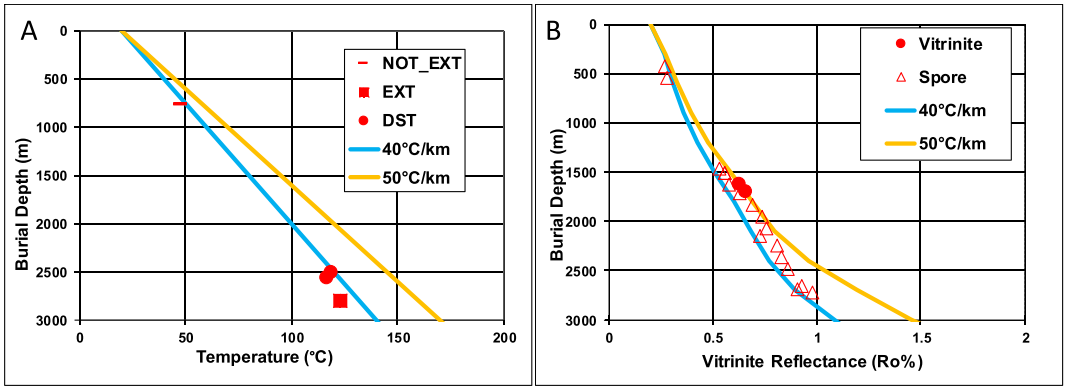

Fig. 3. A) Well A temperature (NOT_EXT = Non extrapolated Log Temperature, EXT = Extrapolated Log Temperature, DST = Production Test Temperature); and B) experimental maturity profile (Vitrinite = Maturity from Vitrinite, Spore = Maturity Ro%eq from spores).

Table 2
Thermochronologic data from apatite fission-track analysis.

Sample number	No. Of crystals	Spontaneous		Induced		$P(\chi)^2$	Dosimeter		Age (Ma) ±1σ	P1	P2
		ρ_s	N_s	ρ_i	N_i		ρ_d	N_d			
S2	21	6.02	532	0.88	602	0.0	0.99	5154	149.5 ± 15.8	91.5 ± 10.7	207.4 ± 16.6
S3	20	13.01	969	1.55	1301	0.0	0.99	4798	141.4 ± 16.6	78.8 ± 5.5	191.9 ± 11.7

to define the organic matter type and a qualitative thermal maturity parameter by visually assessing palynomorph colour (Thermal Alteration Index – TAI). This supports, along with several Tmax data from Rock-Eval pyrolysis (mainly available for the Paleozoic sequence), the vitrinite reflectance method in indicating thermal maturity of the sample.

3.3. Petrography and microthermometric analysis of fluid inclusions

Preliminary to the microthermometric analysis of fluid inclusions (FI), a conventional thin-section petrographic study was performed on selected samples in order to recognize the diagenetic mineral phases occurring in the samples and to detect the relative timing of observed diagenetic events.

After this, the microthermometric analysis of fluid inclusions trapped in cements was performed. The microthermometric analysis was applied to aqueous fluid inclusions of primary origin. These fluid inclusions are two-phase fluid + vapor (L + V), in most cases rare and of small size in the order of 1–5 μm. The microthermometric measurements were performed on double-polished 60 micron-thick thin sections impregnated with blue epoxy resin; a preliminary observation under U.V. light was also executed to detect possible fluorescent hydrocarbon inclusions.

Measurements were done using a Linkam THMS600G heating-freezing stage. Its thermocouple was calibrated using synthetic pure water and CO_2 inclusions. Low heating rates were used for measuring homogenization temperatures (T_h), which were completed following the order of increasing homogenization temperatures to avoid overheating. T_h is considered as a measure of the minimum temperature of crystallization of the diagenetic mineral hosting the inclusions, i.e. the T of the rock at the moment of cement precipitation. Low temperature phase changes were measured after all homogenization temperatures in the sample. Most homogenization temperatures and final ice melting

temperatures (T_m) were measured by cycling (Goldstein and Reynolds, 1994). This measurement (T_m) is used to interpret the bulk salinity of the fluid inclusions, within certain limits because of the unknown complex composition of diagenetic fluids. This is the reason why salinity is expressed in term of % NaCl equivalent, i.e. assuming that the NaCl is most abundant dissolved salt in a NaCl–H2O system. Considering this limitation, the salinity of inclusions was calculated starting from the T_m according to the formula proposed by Bodnar (1992).

3.4. Fission tracks and (U–Th)/He in apatites

Fission-track (AFT) and (U–Th)/He analyses (AHe) on apatite detrital grains were done in order to verify the thermal history of the sedimentary succession with an independent method and to put constraints for the age of thermal events.

Samples were processed using standard procedures, modified according to the small amount of available material. After crushing with a jaw mill, crystals were separated by magnetic (Franz) and heavy-liquid (Na-politungstate) techniques.

Mounts of apatite in epoxy were ground and polished to expose planar surfaces within the grains and then etched with 5 N HNO_3 at 20 °C for 20 s to reveal spontaneous fission-tracks. Samples then were irradiated with thermal neutrons in the reactor at the Radiation Center of Oregon State University with a nominal neutron fluence of 9×10^{15} n cm^{-2}. The CN-5 dosimeter was used to measure neutron fluence. After irradiation, induced fission-tracks in the low-U muscovite that covered apatite grain mounts and glass dosimeter were revealed by etching in 40% HF at 20 °C for 40 min. Apatite FT dates were calculated using the external-detector and the zeta-calibration methods (Hurford and Green, 1983) with IUGS age standards (Durango, Fish Canyon, and Mount Dromedary apatites) (Hurford, 1990) and a value of 0.5 for the $4\pi/2\pi$ geometry correction factor. The analyses were subjected to the $\chi 2$ test (Galbraith, 1981) to detect whether the data sets contained any extra-Poissonian error.

The apatite concentrate has been then carefully examined at a stereoscope equipped with a videocamera under transmitted and reflected light in order to select crystals suitable for (U–Th)/He analysis. The grains should have a section >60 μm, euhedral shape, no fractures parallel to the c axis, no inclusions and no coating. As a whole, 21 crystals have been prepared for the analysis, because they were the only suitable for the analysis, and in other samples no one has been found. Samples have been analyzed at the Institute of Rock Structure and Mechanics of the Czech Academy of Science through the Alphachron (ASI Instruments). Samples are first degassed under vacuum by heating with a Nd-YAG laser. Then concentration of ^4He is determined by ^3He isotope dilution and measurement of the $^4He/^3He$ ratio through an Alphachron quadrupole mass spectrometer. U, Th and Sm concentrations are finally obtained by isotope dilution using an inductively coupled plasma mass spectrometer.

3.5. Thermal models

The thermal model of the basin was developed utilising the Petroleum System Modelling package Simba as a function of the regional geological model developed by Eni.

Simba (e-simba) is a software created by ENI for 1D to 3D modelling that allows a geological model to simulate the processes of HC generation, expulsion and retention. In the pressure/temperature model, the fluid flow evolution in time and space is computed. This is obtained by solving, at each time step of the simulation, a system of partial differential equations that are obtained by combining Darcy's law with the mass balance equations of fluid and solid phases. The temperature distribution is then computed, considering the conductive effects due to the heat flow coming from the basement/sediment interface and the 3D conductivity distribution. The 3D advective effects are also considered calculating the heat distributed by fluid. The physical and chemical processes described by non-linear partial differential equations are discretized by the Finite Element Method on a reference system fixed with respect to the sediment matrix. Time discretization is performed with a fully implicit backward difference scheme. Space discretization is performed with hexahedral 8-node and 20-node finite elements. Convective terms in the temperature equation are handled with the Reverse Particle Tracking Technique. To solve the linear system and compute the solution, e-simba uses the numerical scheme of Preconditioned Conjugate Gradient Method. During the first calibration simulation, the present pressure regime and the present temperature distribution calculated are compared to measure values to calibrate the input data. The software first allows creation of a geological/geometrical model based on chronostratigraphic and structural inputs. Then petrophysical, thermal and geochemical inputs provide an integrated geological/thermal model that traces back through time temperature, pressure, generation, retention patterns.

To the aim of the present work, we tested 3 different thermal scenarios: 1) a heating only due to burial with constant heat-flow; 2) a heating due to burial and an Early Tertiary thermal overprint, with a short-lived event and a doubled heat flow centred at 65 Ma; 3) a heating due to burial with a Late Tertiary thermal overprint, with a short-lived event with doubled heat flow centred at 5,4 Ma. By contrast we did not test a possible pre-Hercynian burial heating because seismic data nearby well location show or null or low angle degree layer dipping below Hercynian Unconformity, suggesting only some tens of meter erosion not recordable by vitrinite reflectance.

4. Results

4.1. Maturity profiles of organic matter and thermal modelling

The well standard thermal experimental data (temperature and vitrinite reflectance) show a general setting in the study area. The maturity trend suggests a paleo-thermal gradient ranging around 50 °C/km while the present thermal gradient is ranging around 40 °C/km (Fig. 3).

This means that in the past the basin was characterized by a greater thermal state possibly due to burial and/or changes of the geothermal gradient. The postulation of a greater past burial is suggested by the presence of the Hercynian Unconformity with Triassic deposit lying directly on Paleozoic sediments. This surface is located around 1000 m burial depth in well A where the organic matter maturity profile was obtained, but the experimental data do not show the classical gap in the maturity profile between samples below and above the surface, also consistent with seismic data nearby the well location which show null or low angle degree layer dipping below Hercynian Unconformity. This suggest only a few tens of meter of erosion, not recordable by vitrinite reflectance. These features led us to interpret the thermal effect of the Hercynian erosion as negligible or overwritten by the Mesozoic burial and thermal histories. The continuity of the maturity profile suggests also that the paleo-thermal event was affecting the entire sampled sedimentary sequence. A Paleozoic important thermal peak would generate a strong slope change in the maturity profile at Hercynian Unconformity, and this seems to be absent. The top-most samples, located around 500 m depth, derive from the Continental "Intercalaire" formation dated at Upper Cretaceous time, and as a consequence of that, the thermal event we are discussing about has to be younger than Upper Cretaceous.

In the shallower sequence contains only few maturity data however, independently from the postulated thermal histories they are matched with, they refer to the cretaceous Continental Intercalaire. The lithology change between Mesozoic and Paleozoic sequence is not so dramatic to justify a maturity slope change, and the presence of some salt layers within the Jurassic sequence does not impact on the general thermal conductive profile because the layers are relatively thin, in the order of some tens of meter.

From these experimental evidences, we argue that a thermal event

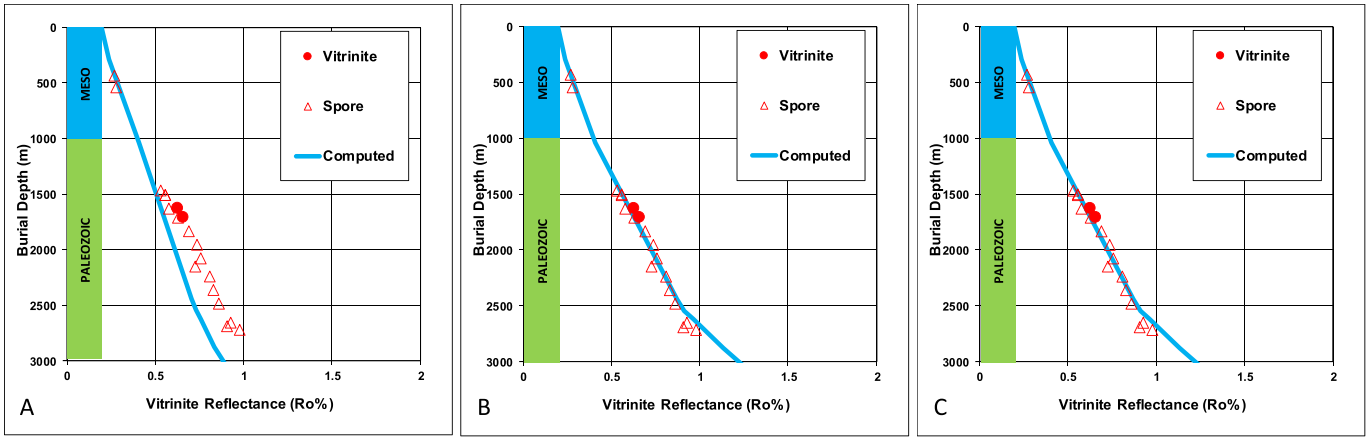

Fig. 4. Experimental maturity profile of organic matter in Well A compared to the maturity profiles predicted by the 3 tested thermal scenarios. A) Without any Tertiary overheating; B) with an Early Tertiary (65 Ma) overheating; C) with a Late Tertiary (5.4 Ma) overheating.

should have happened after the latest Mesozoic burial. Accordingly, we decided to investigate 3 different thermal scenarios (Fig. 4A-B-C). The first scenario simply aims to assess what it should have been expected in the case of simple progressive heating due to increasing burial depth under constant heat flow. This is considered non-realistic for the reasons explained above, but it was still accounted as a useful end-member for detecting the possible heating effect of Tertiary magmatism. The other two scenarios should be considered as the two end-members of the possible thermal effect distribution related to the volcanic activity within the area during Tertiary time (e.g. Liegeois et al., 2005; Rougier et al., 2013).

The results of the 3 simulations suggest, from one side the necessity of a recent heating event to match the Mesozoic maturity gradient (Fig. 4A), to the other the vitrinite data are not enough to discretize the timing of the thermal peak within Tertiary time. As a matter of fact, independently from the age of the thermal pulse, the computed maturity profile is always the same in the case of a lower or upper Tertiary thermal event, i.e. the two simulated end-members (Fig. 4B–C).

4.2. Diagenetic timing and fluid inclusion microthermometry

In order to better constrain the thermal history of the studied reservoir rocks and to link this history to the diagenetic post-depositional modifications suffered by the rocks, the petrographic study on reservoir sandstone samples was first devoted to establish a relative chronological order to the observed diagenetic processes. Afterwards, the microthermometric analysis of primary aqueous fluid inclusions trapped in diagenetic minerals was used to place the different cements along the diagenetic and thermal history of the host rocks, and to get some constraints about the salinity of the diagenetic fluids from which each cement phase precipitated. For the present study, the microthermometric analysis was applied to fluid inclusions occurring along the boundary between grains and quartz overgrowths (QzOvr-boundary), within the overgrowths (QovrInside), in calcite and ankerite cements, and - where present - some measures were obtained also from fluid inclusions in feldspar overgrowths, both along the grain-overgrowth boundary (FOvrBoundary) and within the overgrowths (FOvrInside). As a whole, more than 500 double measures (T_h and T_m) were collected (Fig. 4) and reported in the Data repository (Table DR-1).

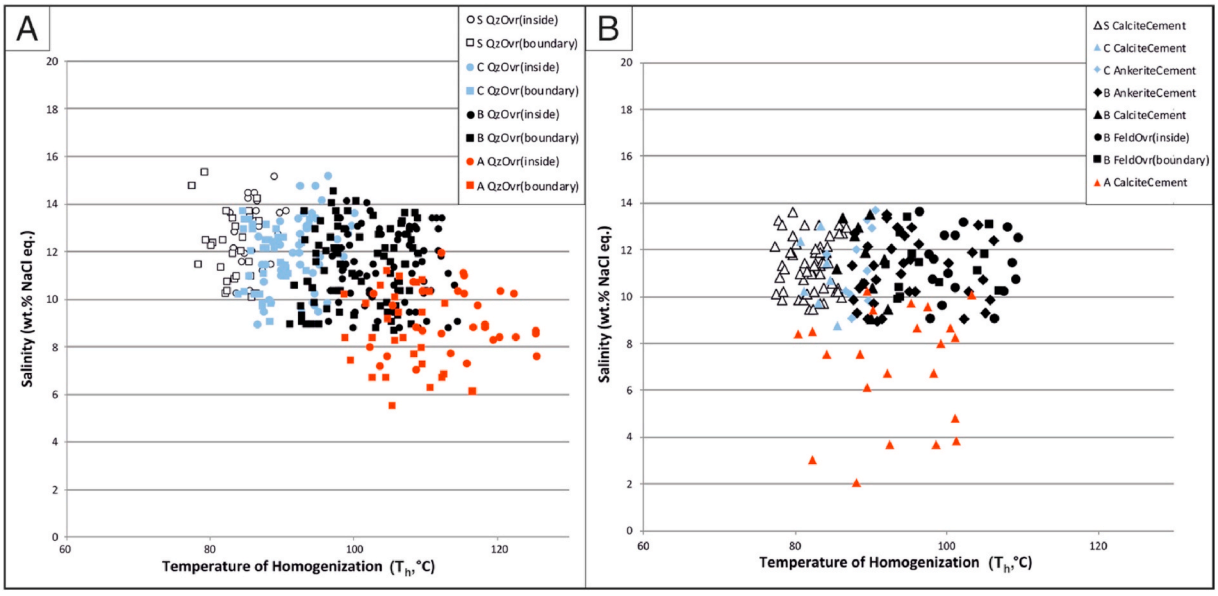

Fig. 5. Th vs. Tm plot obtained for analyzed fluid inclusions in the diagenetic phases occurring in the studied samples. A) fluid inclusions in quartz cement (distinguished in inclusions along the grain-overgrowth boundaries and inside the overgrowths); B) fluid inclusions in Calcite, Ankerite and Feldspar (the latter distinguished in inclusions along the grain-overgrowth boundaries and inside the overgrowths).

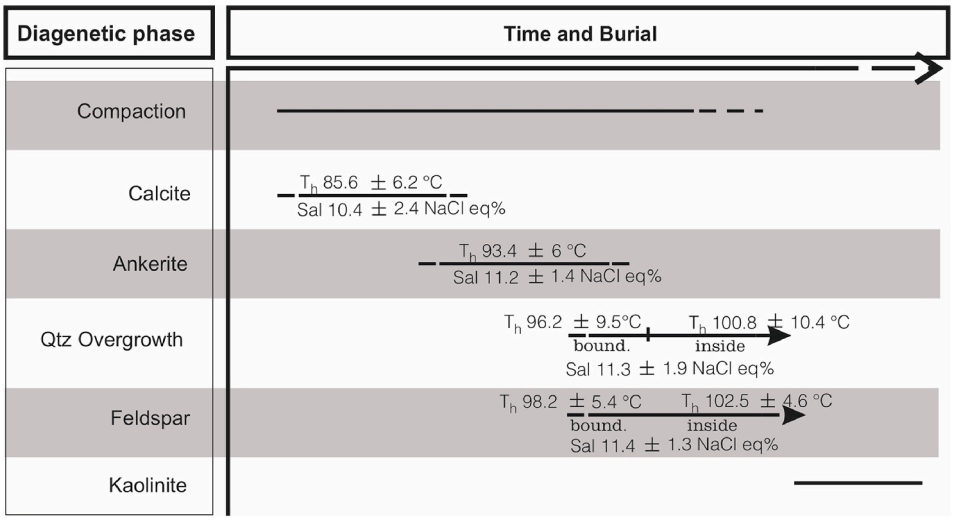

Fig. 6. Diagram summarizing the paragenetic/diagenetic sequence observed in the studied samples, including Th and Tm (average and standard deviation) of primary aqueous fluid inclusions measured in each cement.

In general, the edges between different grains are sparsely interpenetrated or concave/convex, indicative of a moderate degree of compaction and pressure-solution at grain contacts.

In most samples were observed both quartz overgrowths and carbonate cements (Fig. 7A-B-C). Carbonate cements are made by calcite patches (Fig. 7A) and isolated ankerite crystals (Fig. 7B). The lack of overgrowth around quartz grains in pores filled by calcite patches supports the idea that calcite cement predates quartz overgrowth precipitation in the diagenetic sequence. By contrast the occurrence of quartz overgrowth around grains bounding pores where ankerite crystals precipitated, suggests that ankerite is coeval or at least partially postdate quartz.

In addition, there were observed some sparse overgrowth around feldspar grains (Fig. 7D) and kaolinite cements filling pores yet reduced

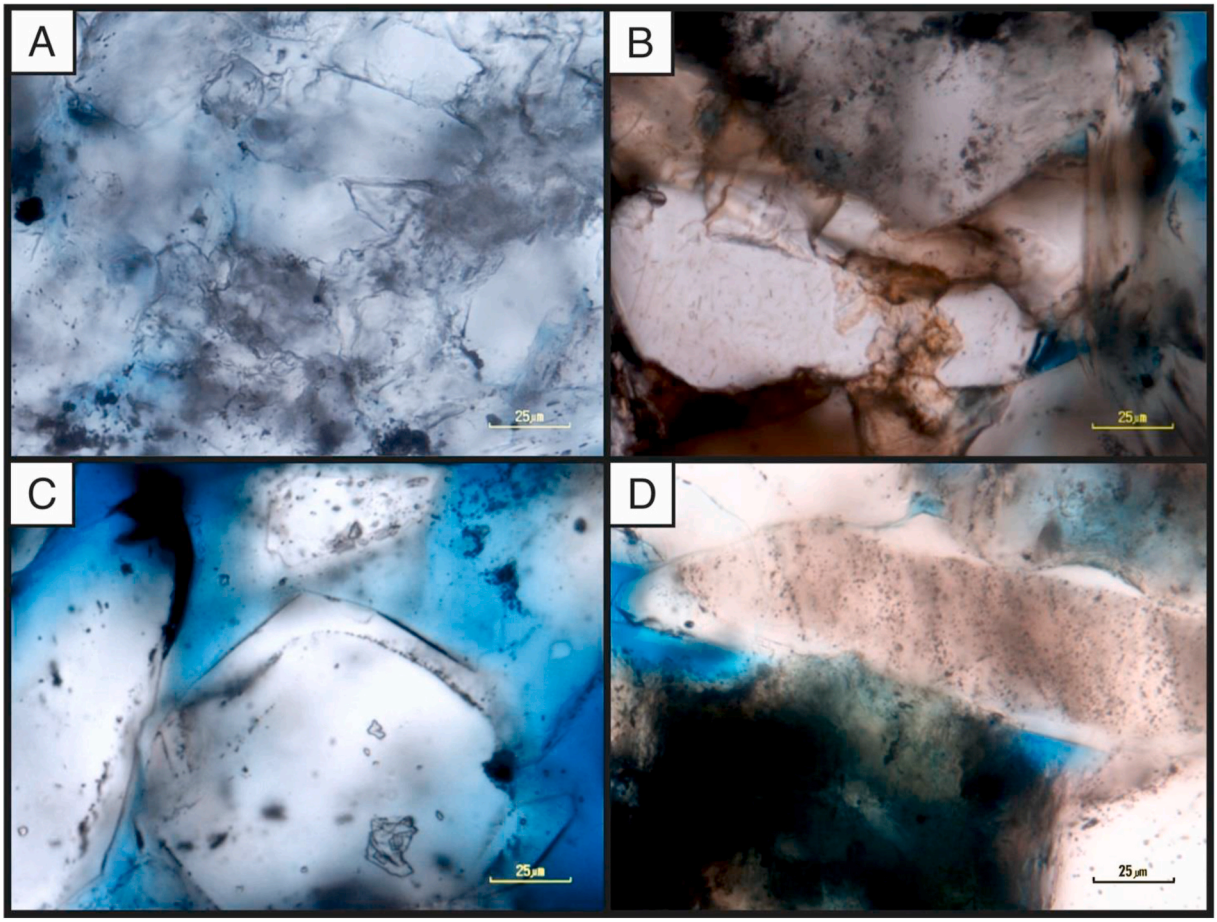

Fig. 7. Photomicrographs of major diagenetic phases occurring in the studied reservoir rocks. A) Calcite patches; B) Ankerite crystals; C) Quartz overgrowth; D) Feldspar overgrowth. Scale bar 25 µm in all pictures.

by quartz growth (Fig. 6G).

Microthermometric measurements worked out that calcite is the cooler phase precipitated (Fig. 5), followed by ankerite plus quartz and feldspar, with kaolinite at the end of the sequence (according to petrographic observations, but no microthermometric measurements were possible in kaolinite crystals). Salinity of fluids trapped in most cement types falls in a quite narrow range around 10–12% NaCl eq., even if some sparse low-salinity inclusions were observed in A1 and A4 samples possibly due to leakage and refilling. This homogeneity suggests a possible common origin of diagenetic fluids for all observed diagenetic phases.

In most cases, well-developed quartz overgrowths were observed, generally with clear separation from the detrital grains due to concentrations of fluid inclusions along the grain-overgrowth boundary (Fig. 7A); the occurrence of primary fluid inclusions along the boundary and within the overgrowth allows to measure the T_h and T_m trends during quartz precipitation. The result of that measures points out that quartz overgrowth precipitated during increasing temperature from around 96 °C to more than 100 °C as an average (Fig. 5; for measures see DR1). In addition, in one of the studied well (well C), illite crystals directly covering quartz grains or forming a rim within quartz overgrowth were observed. In the last case, two different phases of quartz overgrowth precipitation can be distinguished, divided by a quartz + illite rim. Even in this case, an increasing precipitation temperature was obtained during progressive quartz precipitation, with post-illite quartz having a T higher than pre-illite quartz.

Within this overall diagenetic picture, the possibility to analyze samples coming from a quite wide range of burial depth gives the opportunity to study the relations of precipitation temperature of different mineral phases and salinity of trapped fluids, compared to the present-day burial depth. With this respect, a clear correlation is observed between the precipitation temperature of quartz cement and the burial depth of hosting samples, with the only exception of samples coming from well C which have T_h similar to shallower samples from other wells. This contrasts with the markedly constant salinity of trapped fluids (Fig. 8A) and a similar result was obtained also for carbonate cements (Fig. 8B). To account for the difference in precipitation temperature compared with the stratigraphic distance of samples (around 20 °C for a 1.6 km difference in present day depth), by far smaller than what could be expected in a static situation for a common geothermal gradient, we suggest an arrival of diagenetic fluids from a deeper zone, during progressively increasing burial.

With respect to this general picture, samples from well A seem to record a possibly different story, and it is interesting to note that they provided similar results to those reported by English et al. (2016).

Whatever the case, to the aim of the present work focused on the thermal history of the studied samples and not on the modelling of the flow of diagenetic fluids, it is important highlight that the microthermometric analyses document relatively high precipitation temperature (more than 85 °C) even for younger (above Hercynian Unconformity) and shallower (around 2200 m present-day depth) samples.

4.3. Constraints from apatite fission-track and (U–Th)/He ages

An attempt for constraining the thermal history of the studied reservoir rocks was done by means of thermochronologic analysis of apatite grains. Unfortunately, as a whole, both AFT and AHe ages show a large variety of ages (Tables 2 and 3). The two samples dated with AFT analysis yield very similar central ages but, in both the cases, the χ^2 test is failed, thus revealing a significant spread of single grain ages. In fact, although only 21 (sample S2) and 20 (sample S3) crystals could be dated, binomial peak-fitting statistics indicate the presence of two age populations (Late Cretaceous and Early Jurassic).

Distribution of AHe ages across the five samples is more complex, also due to the fact that very few crystals suitable for dating could be found. Age dispersion is generally controlled by the interplay of several factors as shown by the lack of correlation between dates and parameters such as grain radius, eU, [Th], [U], [Sm]. Sample S2 yielded three very similar ages (between 4.3 and 4.7 Ma). A fourth crystal gave an age of 7.0 Ma but, because of its very high U and Sm content, its age is not fully reliable and therefore this crystal will be not considered for discussion. Results for sample S3 are very coherent for two crystals, as they yield ages of 2.4 and 3.0 Ma. The remaining two crystals show much older ages (29.7 and 144.1 Ma) that are probably due to very typical

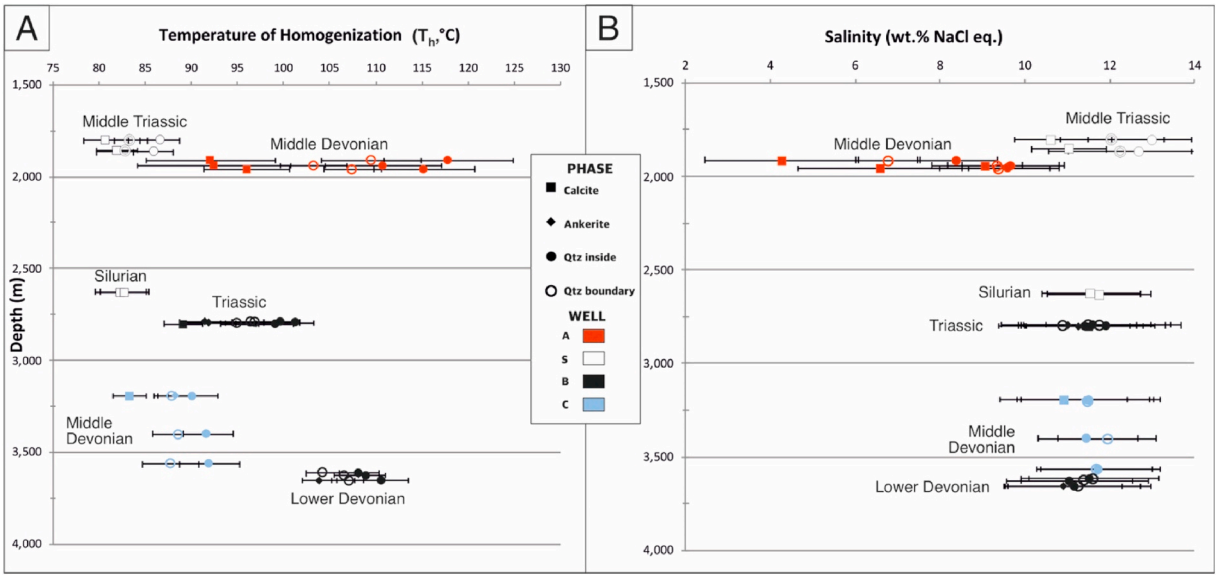

Fig. 8. Precipitation temperature (Th) (A) and salinity of trapped fluids (B) for quartz and carbonate (calcite and ankerite) cements vs. present-day burial depth of studied samples. For each phase, in each well an average and a standard deviation bar is reported. Note as a correlation exists between Th and burial depth, while salinity deduced from Tm is remarkably similar for different phase, wells and burial depth. Well A in partly anomalous from both points of view.

issues such as the presence of inclusions and coating, actually not clearly visible at the microscope. As for sample S2, we will consider only the crystals with younger ages. Sample B3 yielded 4 crystals with a broad

Table 3
Thermochronologic data from apatite (U–Th)/He analysis.

Sample_ grain no.	raw age (Ma)	±σ (Ma)	U (ppm)	Th (ppm)	Sm (ppm)	^{4}He (moles)	eU (ppm)	FT	fully FT correct. Age (Ma)	±σ (Ma)
S2_Ap1	2.50	0.04	23.3	88.5	32.8	3.42E-15	44.1	0.58	**4.3**	0.1
S2_Ap2	3.00	0.23	39.9	34.9	26.1	7.68E-15	48.1	0.64	**4.7**	0.4
S2_Ap3	4.02	0.17	151.8	98.4	675.9	2.01E-14	174.9	0.58	**7.0**	0.3
S2_Ap4	2.51	0.08	36.9	55.4	43.7	3.95E-15	49.9	0.58	**4.4**	0.1
S3_Ap1	92.50	1.17	25.5	74.0	68.2	2.00E-13	42.8	0.64	**144.1**	1.8
S3_Ap2	20.00	1.13	162.8	41.0	68.3	2.50E-13	172.4	0.67	**29.7**	1.7
S3_Ap3	1.66	0.02	86.9	147.9	68.8	1.83E-14	121.7	0.69	**2.4**	0.0
S3_Ap4	1.90	0.03	27.2	76.1	18.4	6.03E-15	45.1	0.64	**3.0**	0.1
B3_Ap1	0.26	0.00	37.2	33.5	16.1	1.94E-15	45.1	0.73	**0.4**	0.0
B3_Ap2	0.73	0.02	47.4	50.6	7.2	2.47E-15	59.3	0.60	**1.2**	0.0
B3_Ap3	3.84	0.12	40.6	20.9	86.4	2.61E-14	45.5	0.71	**5.4**	0.2
B3_Ap4	3.65	0.17	30.6	20.8	31.0	1.09E-14	35.5	0.68	**5.3**	0.3
B5_Ap1	220.30	2.31	3.5	53.1	2.9	6.30E-13	15.9	0.73	**301.4**	3.2
A2_Ap1	1262.64	49.36	1.3	3.0	0.3	6.44E-13	2.0	0.79	**1602.3**	62.6

range of ages, ranging from 0.4 Ma to 5.4 Ma. In this case, the analytical parameters alone do not allow an a priori rejection of one or more ages. We could identify only one suitable crystal in sample B5. The obtained age is much older than the previously described crystals and yields a peculiar low U content. Any judgement of the reliability of this age is not possible because of the lack of any comparison with other grains; this sample will be therefore not considered for discussion. A similar situation has been detected on sample A2 in which only one crystal was analyzed and it gave a very old age. The very low content in U and Th (and, consequently, the low eU) makes the reliability of these data quite low, as visible also from the high analytical error.

The presence of multiple age populations and, in general, the broad dispersion are strong indications for burial temperatures lower than the thermochronology reset temperature but still comprised in the partial annealing or reset range. The reset degree is particularly low when all the crystals yield ages older than the stratigraphic age. Among the analyzed samples, only S2 and S3 have been dated with (U–Th)/He and fission-track analysis. Both the samples show two fission-track age populations. Although these populations are younger than the stratigraphic age, their presence suggests temperatures not higher than 120 °C (at this temperature most of the tracks are completely reset). On the other hand, these samples yield very young (U–Th)/He ages, thus indicating maximum temperature for sure higher than the reset temperature for the (U–Th)/He system. The range of possible temperatures here obtained perfectly fit maximum temperatures recorded by fluid inclusion data.

Central ages calculated using dosimeter glass CN5 and ζ-CN5 = 345.53 ± 18.45 (analyst M.Z.). ρ_s: spontaneous track densities measured in internal mineral surfaces; ρi and ρ_d: induced and dosimeter track densities on external mica detectors ($g = 0.5$); in bracket the number of tracks; $P(\chi^2)$: probability of obtaining χ^2-value for ν degrees of freedom (where ν = number of crystals-1); a probability >5% is indicative of an homogenous population. P1 and P2 refer to populations obtained by the binomial peak-fitting method (Brandon, 1996).

A better definition of thermal history has been attempted by thermal modelling of thermochronologic data. In this work, we used the program HeFTy (Ketcham, 2005) which allows a comparison of experimental and predicted data obtained by inverse and forward modelling. Here, because the burial history is well known, we focused on timing of basin inversion through (U–Th)/He data as they are more sensitive to date cooling given the burial temperature range. Beyond thermochronological information (i.e. the analytical data), we input the geohistory as deduced by stratigraphy and vitrinite data and the present-day temperature as derived from the regional geothermal pattern. We decided to limit our modelling to a forward approach given the tight constraints provided for the burial segments and the maximum temperature. In other words, the only unknown parameter is related to time at which maximum temperature was achieved, thus making an inverse approach not really meaningful. Results do not show a good fit, considering an Early and a Late Tertiary thermal overprint. In both the scenarios, the predicted (U–Th)/He age is younger than what has been measured. In particular, considering sample S2, the two simulations give very similar ages of about 0.5 Ma, quite far from the 4.4–4.7 Ma measured on three crystals (Fig. 9). The impossibility of a good fit is related to the present-day temperature which is too high to predict ages older than 0.5 Ma. In other words, the input temperature is so high (i.e. well inside the retention temperature interval) that the nearly entire previous thermal path should be hidden by reset processes. This element makes any inversion modelling process useless as there are no chances for a successful output. The most plausible reason that could explain the discrepancy between experimental and modelled results is related to the lack of direct measurements of borehole temperatures in the specific well. As a matter of fact, given that at present the samples are in the temperature range in which diffusion processes are active, a very minor decrease of present-day input temperature (i.e. on the order of 5 °C) would have major effects on the predicted (U–Th)/He ages, which rapidly increase.

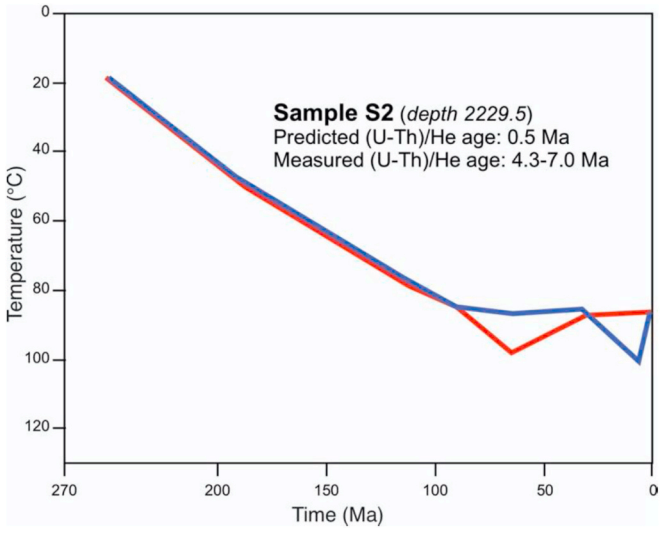

Fig. 9. Forward model obtained by the software HeFTy (Ketcham, 2005) for the sample S2. Blue and red lines indicate two end member scenarios with a late and an early Tertiary thermal peak, respectively. Both thermal paths predict a (U–Th)/He age of 0.5 Ma. The input data derive from stratigraphic, vitrinite and thermal data. (For interpretation of the references to colour in this figure legend, the reader is referred to the Web version of this article.)

5. From temperature to time of cement precipitation: discussion about the predictable age of diagenetic events

The data collected through fluid inclusions microthermometric analyses (T_h) were interpolated with the thermal modelling of studied wells, performed by means of "Simba simulation software", led to estimate the age at which each sample crossed the measured precipitation temperature range, for each diagenetic phase, according to each of the three thermal models tested.

This kind of procedure had a twofold aim: 1) to check if every tested thermal scenario is able to explain all the fluid inclusions experimental data; 2) to test the effects of a chosen thermal model on the predicted precipitation age of cements. Besides the precipitation temperature of each diagenetic phase in each sample, other key factors to be considered are: the burial depth of each sample and the observed trends in the diagenetic sequence, i.e. the order of precipitation, and the fact that quartz precipitated during rock progressive heating (as recorded by systematic difference between T_h at the grain/overgrowth boundary and inside the overgrowths, and not during eventual cooling intervals after temporary overheating).

According to these constraints, the possible age of precipitation was calculated for each phase in each sample for each of the three tested thermal scenarios. The detail of these calculations is reported in the data repository (DR2) whereas a summary of the results of this interpolation is shown in Fig. 10.

From a more comprehensive view of this procedure, it can be worked out that the thermal simulation without any Tertiary overprint fails in explaining a certain number of experimental data; specifically, it fails in explaining the precipitation temperature of the hotter phase (quartz overgrowth) occurring in shallower samples of well S (samples S1 and S3), as well as the precipitation temperature of quartz, feldspar, calcite and ankerite in samples B1-2-3-4. It also partly fails (at least looking at the maximum recorded T_h) in explaining the temperature range of quartz.

Conversely, both simulations including a Tertiary overprint are able to explain all the collected microthermometric data. Nevertheless, the resulting age of each cementation phase is dramatically different in the two simulations. If an Early Tertiary thermal event is assumed, the rocks crossed the precipitation temperature of several cements more than one time (Fig. 10B), thus it is not easy to give a precise age to each cement and a (probable) Cretaceous or a Neogene (less probable) cementation can be predicted. Conversely, if a Late Tertiary thermal event is applied, a Late Cretaceous-Paleogene cement precipitation is obtained. With this respect, thermochronologic data fit fluid inclusions and organic matter proxies from the point of view of maximum temperature reached by the studied samples, suggesting a temperature in between the fission-track and (U–Th)/He reset. Unfortunately, it fails in quantifying precisely the time of last cooling, given the failure of thermal modelling.

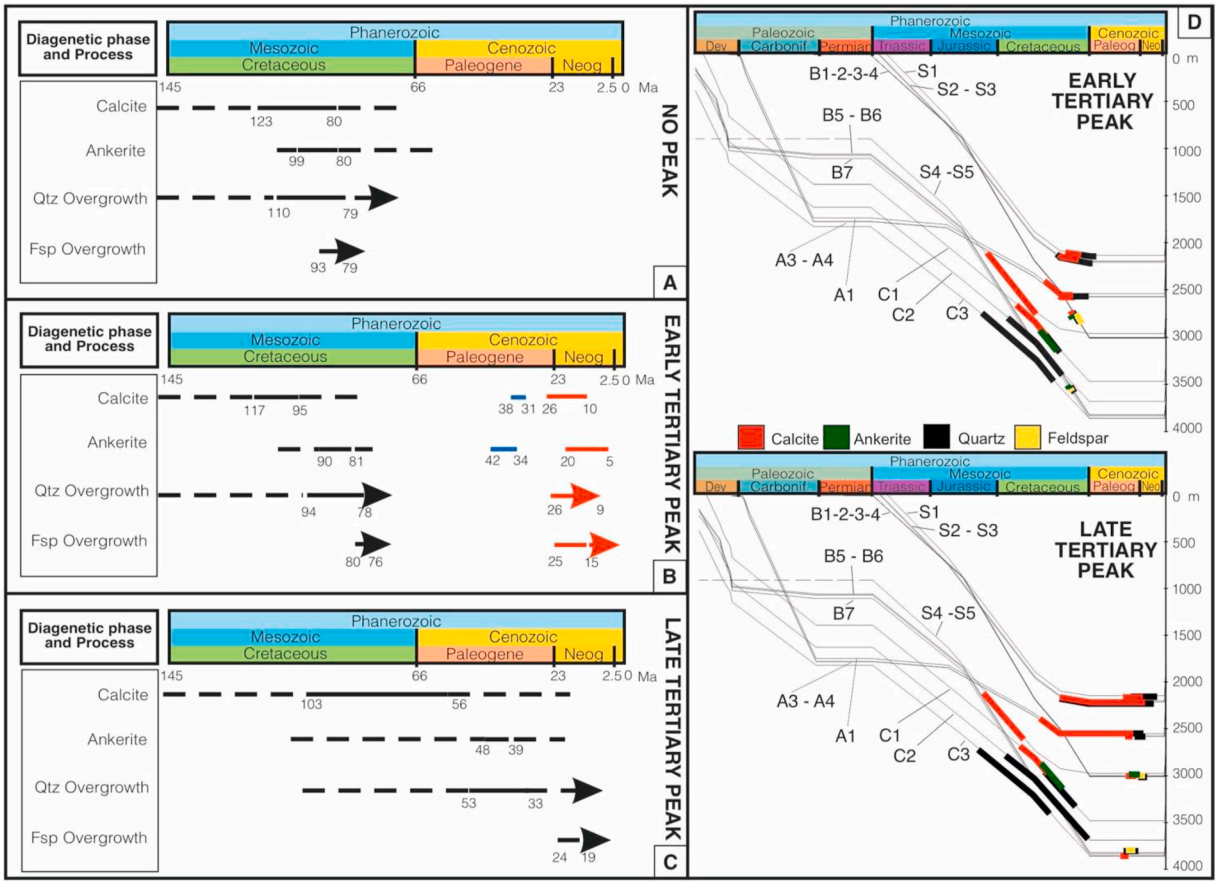

Fig. 10. Predicted age of cement precipitation calculated according the 3 tested thermal scenarios: A) heating only due to burial; B) heating including an Early Tertiary (65 Ma) thermal overprint; C) heating including a Late Tertiary (5.4 Ma) thermal overprint. Arrows refers to diagenetic phases whose precipitation occurred during progressive heating (quartz and feldspar) recorded by increasing Th in the direction of crystal growth. In B blue and red bars report the fact that the samples crossed the precipitation temperatures of cements more than once, during a first heating (black bars/arrows), during the cooling following the Early Tertiary overheating (blue bars) and finally during the new burial-related reheating (red bars/arrows). D) Projection of the calculated time of cements precipitation along the burial history of studied samples according to the thermal scenarios with an Early (top) and a Late (bottom) Tertiary heating. Note that uplift and erosion related to the Hercynian event is considered negligible according to organic matter profile and seismic evidences; see text for further details. Different colors refer to different diagenetic phases: black = quartz; red = calcite; green = ankerite; yellow = feldspar. (For interpretation of the references to colour in this figure legend, the reader is referred to the Web version of this article.)

Therefore, both the scenarios including a Tertiary overheating remain compatible with the collected thermochronology dataset.

6. Conclusions

The new data set collected for the present work contribute to solve the debated problem of the thermal history of the Ghadames-Illizi Basin, deciphering the potential effect of the increase of heat flow related to the magmatic activity occurred in north-west Africa during Tertiary.

The collected data set prove that a simple model with heating only due to burial depth does not explain experimental data; in particular, a significant amount of heating due to burial followed by erosion during Hercynian orogeny cannot be assumed due to the maturity profile of the organic matter across the Hercynian erosional surface. The same result is worked out by fluid inclusion analysis, as precipitation temperature of cements in Triassic reservoir samples (i.e. resting above Hercynian Unconformity) cannot be explained without a post-Mesozoic overheating.

Conversely, a Tertiary overheating is able to account both for organic matter profile and fluid inclusion data. With this respect, between the two tested scenarios including a Tertiary thermal event (with an Early or a Late Tertiary overheating), the simplest case with an Early Tertiary event is also the one that better accounts for all observed data. It must be stressed that two possible end-members reasonable for the real scenario have to be considered. Unfortunately, the attempt to solve completely the problem via apatite low-T thermochronology failed given the lack of precise bore-hole temperature constraints in the studied well and thus demonstrating the critical issues related to the choice of thermal parameters such as the geothermal gradient.

Nevertheless, it is important to note that the geologic time predicted for each phase of cement precipitation occurred in the studied reservoir rocks change quite dramatically (several tens of Ma) depending on the adopted thermal scenario. In addition, our results support the idea that the main phase of cement precipitation in the studied reservoir rocks occurred relatively late, during Cretaceous-Tertiary time. This outcome is clearly different from the Carboniferous age suggested for most of cement precipitation by other authors in other parts of the Illizi Basin (English, 2017a). This obviously has a strong impact on the modelling of diagenesis and evolution of the pore network of Illizi Basin reservoir rocks and emphasizes the need for further investigations to better define their diagenetic story. It is also possible that different parts of the basin experienced different diagenetic pathways, depending on the diverse amount of pre-Hercynian burial and unequal heat flow related to the Tertiary North African magmatic activity.

Credit author statement

Andrea Di Giulio, Domenico Grigo, Massimiliano Zattin and Chiara Amadori conceived the scientific question, defined and performed the work and wrote the manuscript. Chiara Nicola performed the microthermometric analyses. Paolo Scotti performed the vitrinite and spores analyses. Domenico Grigo provided the burial history and thermal simulations. Massimiliano Zattin performed the Apatite Fission Track analyses and thermal modelling. Alberto Consonni and Andrea Ortenzi provided insights to the diagenetic history of studied rocks. Silvia Tamburelli performed the interpolation of the burial and microthermometric data used to date cement phases. All authors contributed to the design of the manuscript and its revision.

Declaration of competing interest

The authors declare that they have no known competing financial interests or personal relationships that could have appeared to influence the work reported in this paper.

Acknowledgements

The authors thank Eni for having provided the studied samples and for permission to publish this paper. Donato Barbieri (Eni) is kindly acknowledged for vitrinite reflectance analysis. This work has been financially supported by Eni and University of Pavia as a part of the PHD project of Silvia Tamburelli. The authors really thank the two unonymous reviewers for their accurate revisions of the manuscript.

Appendix A. Supplementary data

Supplementary data to this article can be found online at https://doi.org/10.1016/j.marpetgeo.2021.104979.

References

Acheche, M.H., M'Rabet, A., Ghariani, H., Ouahchi, A., Montgomery, S.L., 2001. Ghadames basin, southern Tunisia: a reappraisal of Triassic reservoirs and future prospectivity. Am. Assoc. Petrol. Geol. Bull. 85, 765–780. https://doi.org/10.1306/8626C9F1-173B-11D7-8645000102C1865D.

Alpern, B., 1970. Classification petrographique des constituants organiques fossiles des roches sedimentaires. Rev. Inst. Fr. Pet. 25, 1233–1267.

Bertrand, R., 1990. Correlations among the reflectances of vitrinite, chitinozoans, graptolites and scolecodonts. Org. Geochem. https://doi.org/10.1016/0146-6380(90)90102-6.

Bodnar, R.J., 1992. The System H2O-NaCl [abs.]: Biennial PACROFI, 4th, Lake Arrowhead, California, May 22–24, pp. 108–111. Program and Abstracts.

Booth, D.R.D., Clark-Lowes, D.D., Traut, M.W., 1998. Palaeozoic Petroleum Systems of North Africa. Geol. Soc. Spec. Publ. https://doi.org/10.1144/GSL.SP.1998.132.01.02.

Brandon, M.T., 1996. Probability density plot for fission-track grain age samples. Radiat. Meas. https://doi.org/10.1016/S1350-4487(97)82880-6.

English, J.M., English, K.L., Corcoran, D.V., Toussaint, F., 2016a. Exhumation charge: the last gasp of a petroleum source rock and implications for unconventional resources. Am. Assoc. Petrol. Geol. Bull. 100, 1–16. https://doi.org/10.1306/07271514224.

English, K.L., English, J.M., Redfern, J., Hollis, C., Corcoran, D.V., Oxtoby, N., Yahia Cherif, R., 2016b. Remobilization of deep basin brine during exhumation of the Illizi Basin, Algeria. Mar. Petrol. Geol. 78, 679–689. https://doi.org/10.1016/j.marpetgeo.2016.08.016.

English, K.L., Redfern, J., Corcoran, D.V., English, J.M., Cherif, R.Y., 2016c. Constraining burial history and petroleum charge in exhumed basins: new insights from the Illizi Basin, Algeria. Am. Assoc. Petrol. Geol. Bull. https://doi.org/10.1306/12171515067.

English, K.L., English, J.M., Bonnel, L.M., Lander, R.H., Hollis, C., Redfern, J., Guirdham, C., Garnham, J., Cherif, R.Y., 2017a. Controls on reservoir quality in exhumed basins – an example from the Ordovician sandstone, Illizi Basin, Algeria. Mar. Petrol. Geol. 80, 203–227. https://doi.org/10.1016/j.marpetgeo.2016.11.011.

English, K.L., Redfern, J., Bertotti, G., English, J.M., Yahia Cherif, R., 2017b. Intraplate uplift: new constraints on the Hoggar dome from the Illizi basin (Algeria). Basin Res. 29, 377–393. https://doi.org/10.1111/bre.12182.

Galbraith, R.F., 1981. On statistical models for fission track counts. Math. Geol. 13, 471–488. https://doi.org/10.1007/BF01034498.

Galeazzi, S., Point, O., Haddadi, N., Mather, J., Druesne, D., 2010. Regional geology and petroleum systems of the Illizi-Berkine area of the Algerian Saharan Platform: an overview. Mar. Petrol. Geol. https://doi.org/10.1016/j.marpetgeo.2008.10.002.

Goldstein, R.H., Reynolds, T.J., 1994. Systematics of fluid inclusions in diagenetic minerals. SEPM Short. Course 31 (1994), 199. https://doi.org/10.2110/scn.94.31.

Hurford, A.J., 1990. Standardization of fission track dating calibration: Recommentation by Ficcio Track Working Group of I.U.G.S. Subcommission on Geochronology. Tect. Geol.: Isot. Geosci. Sect. 80 (2), 171–178. https://doi.org/10.1016/0168-9622(90)90025-8.

Hurford, J.A, Green, P.F., 1983. The zeta age calibration of fission-track dating. Chem. Geol. 41, 285–317. https://doi.org/10.1016/S0009-2541(83)80026-6.

Ketcham, R.A., 2005. Forward and inverse modeling of low-temperature thermochronometry data. Rev. Mineral. Geochem. 58 (1), 275–314. https://doi.org/10.2138/rmg.2005.58.11.

Liégeois, J.P., Benhallou, A., Azzouni-Sekkal, A., Yahiaoui, R., Bonin, B., 2005. The hoggar swell and volcanism: reactivation of the precambrian Tuareg shield during alpine convergence and West African cenozoic volcanism. Spec. Pap. Geol. Soc. Am. https://doi.org/10.1130/0-8137-2388-4.379.

Macgregor, D.S., 1996. The hydrocarbon systems of North Africa. Mar. Petrol. Geol. https://doi.org/10.1016/0264-8172(95)00068-2.

Rougier, S., Missenard, Y., Gautheron, C., Barbarand, J., Zeyen, H., Pinna, R., Liégeois, J. P., Bonin, B., Ouabadi, A., Derder, M.E.M., de Lamotte, D.F., 2013. Eocene exhumation of the Tuareg shield (Sahara desert, Africa). Geology. https://doi.org/10.1130/G33731.1.

Swezey, C.S., 2009. Cenozoic stratigraphy of the Sahara, northern Africa. J. Afr. Earth Sci. https://doi.org/10.1016/j.jafrearsci.2008.08.001.

Tissot, B., Espitalie, J., Deroo, G., Tempere, C., Jonathan, D., 1984. Origin and migration of hydrocarbons in the eastern Sahara (Algeria). Pet. Geochemistry Basin Eval.

Traut, M.W., Boote, D.R.D., Clark-Lowes, D.D., 1998. Exploration History of the Palaeozoic Petroleum Systems of North Africa. Geol. Soc. Spec. Publ. https://doi.org/10.1144/GSL.SP.1998.132.01.03.

Underdown, R., Redfern, J., 2008. Petroleum generation and migration in the Ghadames Basin, north Africa: a two-dimensional basin-modeling study. Am. Assoc. Petrol. Geol. Bull. https://doi.org/10.1306/08130706032.

Wendt, J., Kaufmann, B., Belka, Z., 2009. Devonian stratigraphy and depositional environments in the southern Illizi Basin (Algerian Sahara). J. Afr. Earth Sci. https://doi.org/10.1016/j.jafrearsci.2009.03.006.

Wilson, M., Guiraud, R., Moreau, C., Bellion, Y.J.C., 1998. Late permian to recent magmatic activity on the african-arabian margin of tethys. Geol. Soc. Spec. Publ. https://doi.org/10.1144/GSL.SP.1998.132.01.14.

Wilson, M., Guiraud, R., 1992. Magmatism and rifting in western and central Africa, from late jurassic to recent times. Tectonophysics. https://doi.org/10.1016/0040-1951(92)90259-9.